ISOLATING WOODY PLANT MATERIAL AND SENESCENT VEGETATION FROM GREEN VEGETATION IN AVIRIS DATA

ROBERTS, D.A., SMITH, M.O., ADAMS, J.B., SABOL, D.E., GILLESPIE A.R. and WILLIS, S.C. Department of Geological Sciences, University of Washington, Seattle, WA 98195

ABSTRACT

Spectral linear mixture analysis was applied to Airborne Visible/Infrared Imaging Spectrometer (AVIRIS) data to calibrate the data to reflectance and distinguish senescent vegetation and woody plant material from green vegetation and soils. The linear mixing model was applied to a data set collected September 20, 1989 over the Jasper Ridge Biological Preserve. The data were successfully calibrated to reflectance resulting in reasonable reflectance spectra for vegetated and unvegetated areas within and in the vicinity of the Preserve. The data were modeled as mixtures of four endmembers: shade, green leaf, soil and a woody endmember. A senescent vegetation endmember that was spectrally distinct from soils could not be reliably modeled but could be distinguished from soils using band residuals calculated as the difference between the measured AVIRIS spectrum and a model consisting of variable fractions of the four endmembers. Positive residuals at wavelengths between 1.5 and 1.7 μm and negative residuals at 2.08 (cellulose) and 2.28 (lignin) μm distinguished senescent plant material from soils.

INTRODUCTION

Considerable research has focussed on quantifying the amount of green vegetation measured remotely. Examples include uses of vegetation indices such as the normalized difference vegetation index (NDVI) and the Perpendicular Vegetation Index (PVI) (e.g., Tucker, 1979 and Jackson, 1983). Other examples include the use of airborne spectrometer data to measure canopy biochemical constituents (Peterson et al., 1987; Goetz et al., 1990).

Considerably less research has focussed on the woody or senescent components, though these can represent a significant portion of the biomass within a canopy or a vegetation community. Huete and Jackson (1987) varied the amount of senescent material and leaf litter relative to green vegetation to determine the effects of these materials on the assessment of green vegetation using vegetation indices. Elvidge (1987) measured visible near-infrared

and thermal spectra of dry plant materials, green leaves and other organic components of California Black Oak (Quercus kelloggii) to assess the potential for the development of vegetation indices designed for the assessment of dry plant materials. Gillespie et al. (1990a) found that dry grass and shrubs, which could not be distinguished from soils using Thematic Mapper (TM) data, could be distinguished using thermal data. Recently Adams et al. (1990), using spectral mixture analysis, found that the spectral variability within TM data collected over Manaus, Brazil, could be best explained by including a wood endmember in addition to green vegetation, shade and soil.

One of the major reasons for the lack of research pertaining to wood and senescent materials is the similarity between the spectra of dry plant materials and soils (Figure 1). Dry plant materials lack the pronounced spectral contrast between near-infrared and red wavelengths that distinguish green plant materials from soils. Thus, using the broad TM bands, it is difficult to distinguish woody plant material from soils and may be impossible to distinguish senescent plant material from soils. AVIRIS, on the other hand, collects data within wavelength regions where there are cellulose and lignin absorption features that can be used to distinguish soils from senescent vegetation or wood (Elvidge, 1987). In order to investigate the applicability of AVIRIS for assessing nongreen biomass, we applied techniques similar to those of Adams et al. (1990).

METHODS

We utilized a linear-mixing approach to model radiance measured by the sensor as the sum of several "pure spectra" (endmembers), each weighted by the relative proportion of the material corresponding to each spectrum within the field of view (Equation 1).

$$\mathbf{DN}_{ik} = \mathbf{g}_i \sum_{j=1}^{n} \mathbf{f}_j \mathbf{r}_{ij} + \mathbf{o}_i + \varepsilon_i \qquad (1)$$

where $\mathbf{DN}_{ik}$ is encoded radiance measured by the sensor, i is the band number, k is the pixel location, j is the endmember number, $\mathbf{f}_j$ is the fraction of the endmember within the field of view, $\mathbf{r}_{ij}$ is the laboratory reflectance for each reference endmember, $\mathbf{g}_i$ is an atmospheric/instrumental/solar gain term, $\mathbf{o}_i$ is an atmospheric/instrumental offset and ε_i is a residual and error term.

The gain and offset terms (g_i and o_i) used to calibrate the AVIRIS data were derived using techniques developed by Smith et al. (1987). Smith et al. used least squares regression to relate laboratory-measured reflectance to encoded radiance and solve for the gains and offsets. A regression coefficient (r^2) was generated for each band to assess the fit between encoded radiance spectra and reference endmember spectra.

An average Root Mean Squared (RMS) error was calculated using equation 2.

$$\mathbf{RMS} = \sum_{k=1}^{m}\left(\sqrt{\left(\sum_{i=1}^{n}(\mathbf{DN}_{ik}-\mathbf{DN}_{ik'})^2\right)/n}\right)/m \qquad (2)$$

where $\mathbf{DN}_{ik}$ refers to modeled radiance and m is the number of pixels comprising the image. An average RMS error for the swath used in the analysis was generated to provide a measure of how much of the spectral variability was explained by the endmembers used in the analysis. An RMS error image was generated to show the spatial distribution of the error.

Fraction images for each endmember were produced. Band residuals (ε_i) were calculated by subtracting modeled radiance, predicted for each pixel from the fractions of the endmembers and the gains and offsets used to calibrate the data, from encoded radiance measured by the sensor ($\varepsilon_i = \mathbf{DN}_i - \mathbf{DN'}_i$, Figure 2). A positive residual occurs when the measured spectrum has higher reflectance at a specific wavelength than the modeled spectrum, indicating that the modeled spectrum contains absorption features which were lacking in the measured spectrum. A negative band residual results when the opposite is true, indicating the presence of absorption features in the measured spectrum which were absent or less pronounced in the modeled spectrum.

Fractions of woody and senescent plant material were determined both using fraction images and by interpretation of residual images. Residual images were produced for the wavelength regions of 1.5 to 1.7 and 2.1 to 2.3 μm. These regions were selected because of the presence of lignin and cellulose absorption features which could potentially differentiate senescent leaf materials from soils. For more detailed descriptions of the linear-mixing approach used in this study and residual analysis techniques refer to Adams et al. (1990), Smith et al. (1990) and Gillespie et al. (1990b).

The study was conducted over Jasper Ridge, California. The Jasper Ridge Biological Preserve is located in the foothills along the

northeastern margins of the Santa Cruz Mountains, approximately 7 km west of Palo Alto (Figure 3). Elevations at the site ranged from 108 meters at Searsville Lake to 200 meters on the ridge. The1200-acre, 4-km by 2-km preserve was chosen as a study site because it is an area in which the vegetation has been extensively mapped and because large quantities of senescent and woody plant material were present in the Preserve at the time of the overflight.

The AVIRIS data utilized in this study were collected on September 20, 1989. Calibration and analysis were restricted to a subsection of the full scene, consisting of a 112-pixel swath centered over Jasper Ridge (Figure 3). A 171-band subset of the 224 AVIRIS bands, consisting of bands outside of major atmospheric absorption features was used for analysis. (See Slide 1.)

RESULTS

Calibration

We found that most of the variability within the scene could be explained using four reference endmembers: shade, tan soil (T2HA), woody plant material ("red stems") and green leaf (PHAR on Figure 4). The resulting average RMS error was less than 3 DN (Figure 5). The image was calibrated to reflectance using a best-fit linear combination of the four endmembers and equation 1. A plot of the inverted gains used to calibrate the data roughly corresponds to a plot of the solar curve combined with atmospheric absorption (Figure 6). The inverse of the gain differed most from the solar curve at wavelengths less than 1 μm, which may reflect instrumental effects. Offsets ranged as a function of wavelength between values of 90 and 130 DN, averaging approximately 100 DN (Figure 7). An increase to approximately 130 DN at shorter wavelengths represents increased additive path radiance due to atmospheric scattering. Between 2.0 and 2.4 μm, in the wavelength range of data collected by Spectrometer D, the offset term was also high, averaging 120 DN. Across all wavelengths, the offset showed a pronounced alternating pattern between high and low values, a data characteristic that is probably instrumental in origin.

The model fit (r^2) averaged over 0.98 (Figure 8). The lowest r^2 value was 0.80, occurring approximately at 0.7 μm, at the start of the "red edge" of the vegetation spectrum. The close proximity to the red edge suggests that much of the error could be attributed to poor wavelength calibration. Instrumental wavelength calibration was tested for the September 20, 1989 data set (Green et al., 1990) and

found to be within 0.0005 μm, suggesting that a majority of the miscalibration, if present, was in the laboratory reflectance data used to calibrate the scene. Low r^2 values at 1.100,1.400, 1.900 and >2.400 μm are probably due to changes in atmospheric water abundance with elevation across the scene (Green et al., 1989; Gao and Goetz 1990).

Overall calibration of the image to reflectance appeared to be good as judged by the shape of spectra extracted for areas containing known materials. Reflectance spectra were extracted for three areas within the scene ("lawn," "chaparral" and "drygrass," on Figure 9, labeled L, C and D on Figure 3). The overall brightness and shape of these calibrated AVIRIS spectra are close to similar materials measured in the field, though no quantitative comparison was made to evaluate the accuracy of the calibration. Spectral anomalies within the drygrass spectra at 0.7 μm are probably due to wavelength miscalibration. Spectral anomalies at 0.94 μm and 1.130 μm are probably due to differences in atmospheric water abundance. Comparison to the uncalibrated data for these same areas demonstrates a marked improvement in the interpretability of these spectra (Figure 10).

Mixture Analysis

AVIRIS spectra were modeled as mixtures of four endmembers (Figure 4). The fact that the data could be modeled using these four endmembers does not imply that these materials actually occur in the scene. For example, the spectrum T2HA corresponds to a highly reflectant soil collected in Tucson, Arizona. PHAR equals leaf reflectance of Phalaris arundinacea measured in the laboratory. What these endmembers do imply is that there are materials within the scene that have spectral properties similar to the materials used as endmembers and that all of the materials within the scene can be modeled as mixtures of these spectra. Thus, the fact that T2HA is a viable endmember suggests that the spectral properties of some of the soil in the area are similar to T2HA. Phalaris arundinacea worked well as an endmember for vegetation because of its high near-infrared/red contrast. The red stem endmember does not imply that the woody materials in the scene were red stems, only that this endmember was representative of material in the scene which is spectrally similar to wood.

Fraction images were generated for the four endmembers (Figure 11). In all of the fraction images, roads, buildings and man-made structures, such as the Stanford Linear Accelerator (SLAC), appear anomalous. These materials were not included in the model

and therefore model results for areas containing these materials are not meaningful (see also Figure 5). The highest fractions of shade were located at Searsville Lake (W in Figure 3), at several flooded quarries southeast of Jasper Ridge and on the northeast facing slope of Jasper Ridge, in an area dominated by evergreen forest (marked by arrows on Figure 11a). Shade fractions were lowest in an open field north of Jasper Ridge, in an area consisting of exposed soil and flattened, senescent grass (Elvidge, oral communication, 1990). Green leaf (Figure 11b) was highest to the extreme southeast on a well-watered golf course. A second high fraction occurred on the western edge of the Preserve, in an area containing riparian vegetation (S on Figure 3). The lowest fractions of green leaf occurred in the same region containing the flattened grass and exposed soil, along the central crest of Jasper Ridge, in an area dominated by grasslands and serpentine soils, and to the southeast in areas interpreted as grasslands. Soil fractions (Figure 11c) were highest in a series of open fields southeast of the ridge, along the central crest of the ridge and in the exposed area to the north of the preserve. The lowest soil fractions occurred on the northeast-facing evergreen forest. The fraction of the woody material endmember (Figure 11d) was low across most of the scene. Woody material fractions were highest on Jasper Ridge within the grasslands and the chaparral. According to this analysis, the endmember constituted as much as 8% of the grassland areas and 23% within the chaparral. When the shade endmember is not included in the fraction sum, the fraction of the woody endmember will be larger.

Residual Analysis

Spectral mixture analysis of the data produced coherent maps showing the fractions of these four endmembers within the Jasper Ridge scene. However, these fraction images do not effectively separate the senescent leaf material and soils. Based upon personal observations between 1983 and 1985 on the Jasper Ridge Biological Preserve, we are aware that some of the areas which are modeled as having a high soil fraction, in fact contain much higher fractions of senescent vegetation than soil. Spectral similarity between these two materials makes separating them difficult. This problem was further demonstrated during the process of mixture analysis and calibration. While initially processing and calibrating the image, the spectral library used to calibrate the image contained both dry plant material and soils. Whereas a woody material endmember was a necessary component, senescent vegetation was not. The spectrum for senescent vegetation could be modeled as some linear

combination of the woody material, green leaf, soil and shade endmembers.

Although senescent vegetation did not prove to be a viable endmember for mixture analysis, band residuals distinguished the areas containing large quantities of senescent vegetation from those containing soils (Figures 12 and 13). Figure 12 shows band residuals from 1.59 to 1.71 μm. The exposed hill north of Jasper Ridge (arrow at bottom of figure), the grassland along the crest of the ridge and areas southeast of the ridge show as positive anomalies (see also Figure 2). In the 2.04 to 2.22 μm residual image (Figure 13), these same areas are shown as prominent negative anomalies. The positive anomaly between 1.5 to 1.7 μm corresponds to a spectral region where the measured spectrum has higher reflectance than the modeled spectrum. A comparison between the reflectance spectrum of dried Phalaris arundinacea and the modeled spectrum for the area labeled as drygrass shows an overall positive anomaly with subtle spectral highs at 1.55 and 1.64 μm (Figure 14). Band residuals of the AVIRIS data between 1.588 and 1.706 μm show the highest positive residual at 1.647 μm. The negative anomaly between 2.1 and 2.3 μm corresponds to a spectral region where the measured spectrum had lower reflectance than the model. A comparison between the dried Phalaris spectrum and the modeled spectrum (Figure 14), shows two regions centered at 2.083 μm and 2.291 μm where the Phalaris spectrum contains absorption features not present in the model. The wavelength of these features suggests that the 2.08 μm absorption is due to cellulose and the 2.29 μm absorption is due to lignin (Elvidge, 1987). Using a residual approach, materials that could not readily be modeled as endmembers could be observed as residuals.

SUMMARY

The mixing model was used to successfully calibrate AVIRIS data to reflectance. An AVIRIS scene collected over Jasper Ridge on September 20, 1989 was modeled as consisting of four spectral endmembers: shade, tan soil (T2HA), green leaf (PHAR) and woody material ("red stems"). Although senescent grass could not readily be separated from soil as an endmember, residuals in the 1.5- to 1.7-μm, and 2.1- to 2.3-μm region made it possible to map regions containing high fractions of senescent plant material.

ACKNOWLEDGMENTS

This research was supported by the Land Processes Branch of the National Aeronautics and Space Administration and the W.M. Keck Foundation. We also thank the Jet Propulsion Laboratory for supplying AVIRIS data, and Dr. David Mouat for plant material supplied by him.

REFERENCES

Adams, J.B., Kapos, V., Smith, M.O., Almeida F.R., Gillespie, A.R., and Roberts, D.A., 1990, A New Landsat View of Land use in Amazonia, Proc. of the Int. Symp. Primary Data Acquisition, Manaus, Brazil, June 24-29, 1990, pp. 177-185.

Adams, J.B., Smith, M.O. and Gillespie, A.R., 1990, Imaging Spectroscopy: Data Analysis and Interpretation Based on Spectral Mixture Analysis, in Remote Geochemical Analysis: Elemental and Mineralogical Composition (Pieters and Englert Eds.), in press.

Elvidge, C. D., 1987, Reflectance Characteristics of Dry Plant Material, Presented at the twenty-first International Symposium on Remote Sensing of Environment, Ann Arbor, MI, Oct. 26-30, 1987, 13 pp.

Gao, B-C and Goetz, A.F.H., 1990, Column Atmospheric Water Vapor Retrieval from Airborne Spectrometer Data, *J. Geophys Res. - Atmos.* , in press.

Gillespie, A.R., Smith, M.O., Adams, J.B., and Willis, S.C., 1990a, Spectral Mixture Analysis of Multispectral Thermal Infrared Images, Proc. Airborne Science Workshop: TIMS, Jet Propulsion Laboratory, Pasadena, CA, June 6, 1990. In this volume.

Gillespie, A.R., Smith, M.O., Adams, J.B., Willis, S.C., Fischer, A.F. III and Sabol, D., 1990b, Interpretation of Residual Images: Spectral Mixture Analysis of AVIRIS Images, Owens Valley, CA, Proc. Airborne Science Workshop: AVIRIS,In this volume.

Goetz , A.F.H., Gao, B-C., Wessman, C.A. and Bowman, W.D., 1990, Estimation of Biochemical Constituents from Fresh Green Leaves by Spectrum Matching Techniques, Proc. 10th Annual Int Geosci. Rem. Sens. Symp., College Park, Md, May 20-24, 1990, pp. 971-974.

Green, R.O., Carrere, V., and Conel, J.E., 1989, Measurement of Atmospheric Water Vapor Using the Airborne Visible/Infrared Imaging Spectrometer, Proc. 12th Workshop on Image Processing, ASPRS, in press.

Green, R.O., Conel, J.E., Bruegge, C., Carrere, V., Margolis, J., and Hoover, G., 1990, Laboratory Spectral and Radiometric Calibration of AVIRIS, Proc. Airborne Science Workshop: AVIRIS, Jet Propulsion Laboratory, Pasadena, CA, June 4-5, 1990, In this volume.

Huete A.R. and Jackson, R.D., 1987, Suitability of Spectral Indices for Evaluating Vegetation Characteristics in Arid Rangelands, *Rem. Sens. Environ.*, 23:213-232.

Jackson, R.D., 1983, Spectral Indices in n-space, *Rem. Sens. Environ.*, 13:409-421.

Peterson, D.L., Aber, J.B., Matson, P.A., Card, D.H., Swanberg, N., Wessman, C. and Spanner, M., 1988, Remote Sensing of Forest Canopy and Leaf Biochemical Contents, *Rem. Sens. Environ.*, 24:85-108.

Smith, M.O., Roberts, D.A., Shipman, H.M., Adams, J.B., Willis, S.C. and Gillespie, A.R., 1987, Calibrating AIS images using the surface as a reference, Proc. 3rd Airborne Imaging Spectrometer Data Analysis Workshop, June 2 - 4, 1987, 10 p.

Smith M.O., Ustin, S.L., Adams, J.B. and Gillespie, A.R., 1990, Vegetation in Deserts I. A Regional Measure of Abundance for Multispectral Images, *Rem. Sens. Environ.*,31:1-26.

Tucker, C.J., 1979, Red and Photographic Infrared Linear Combinations for Monitoring Vegetation, *Rem. Sens. Environ.*, 8:127-150.

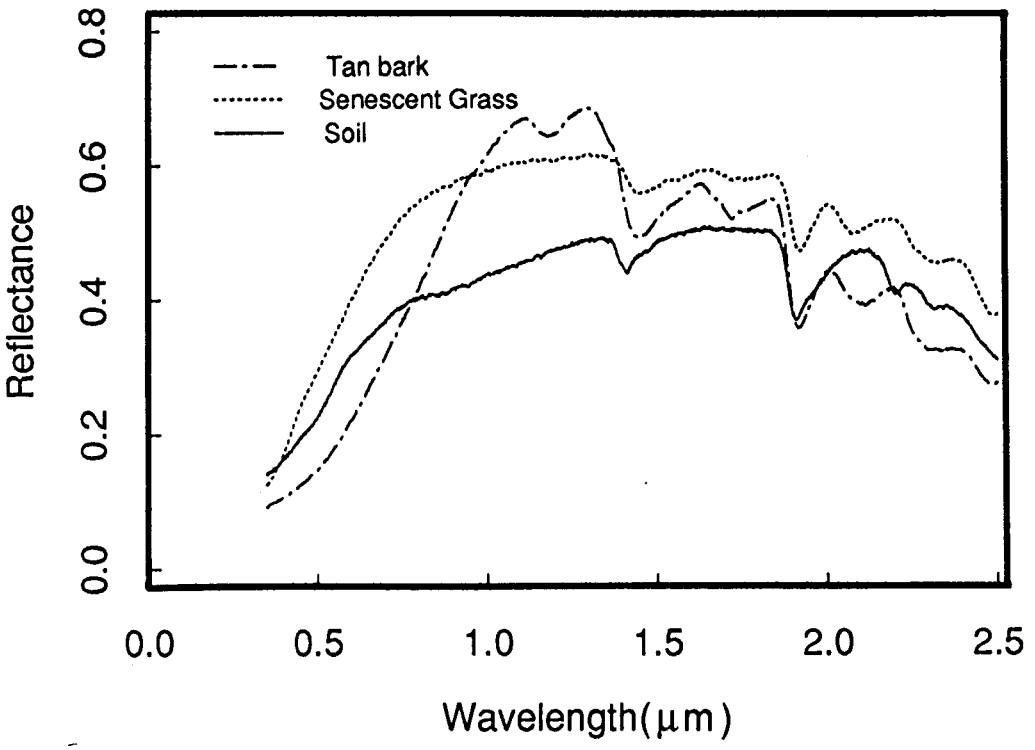

Figure 1. Reflectance spectra of tan bark (Platinus sp.), senescent grass (Phalaris arundinacea) and a soil. Note the spectral similarity, particularly between the senescent grass and the soil.

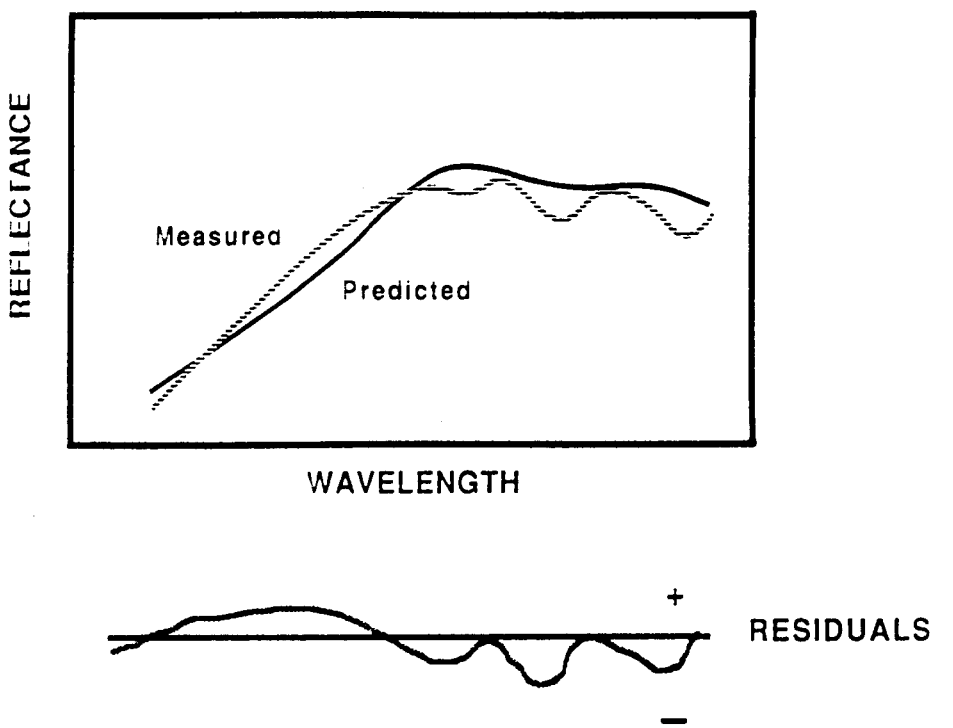

Figure 2. Comparison of measured reflectance (dashed) to modeled reflectance (solid). Subtraction of the predicted from the measured spectrum results in positive residuals when the measured value is higher than the model and negative residuals when the opposite is true.

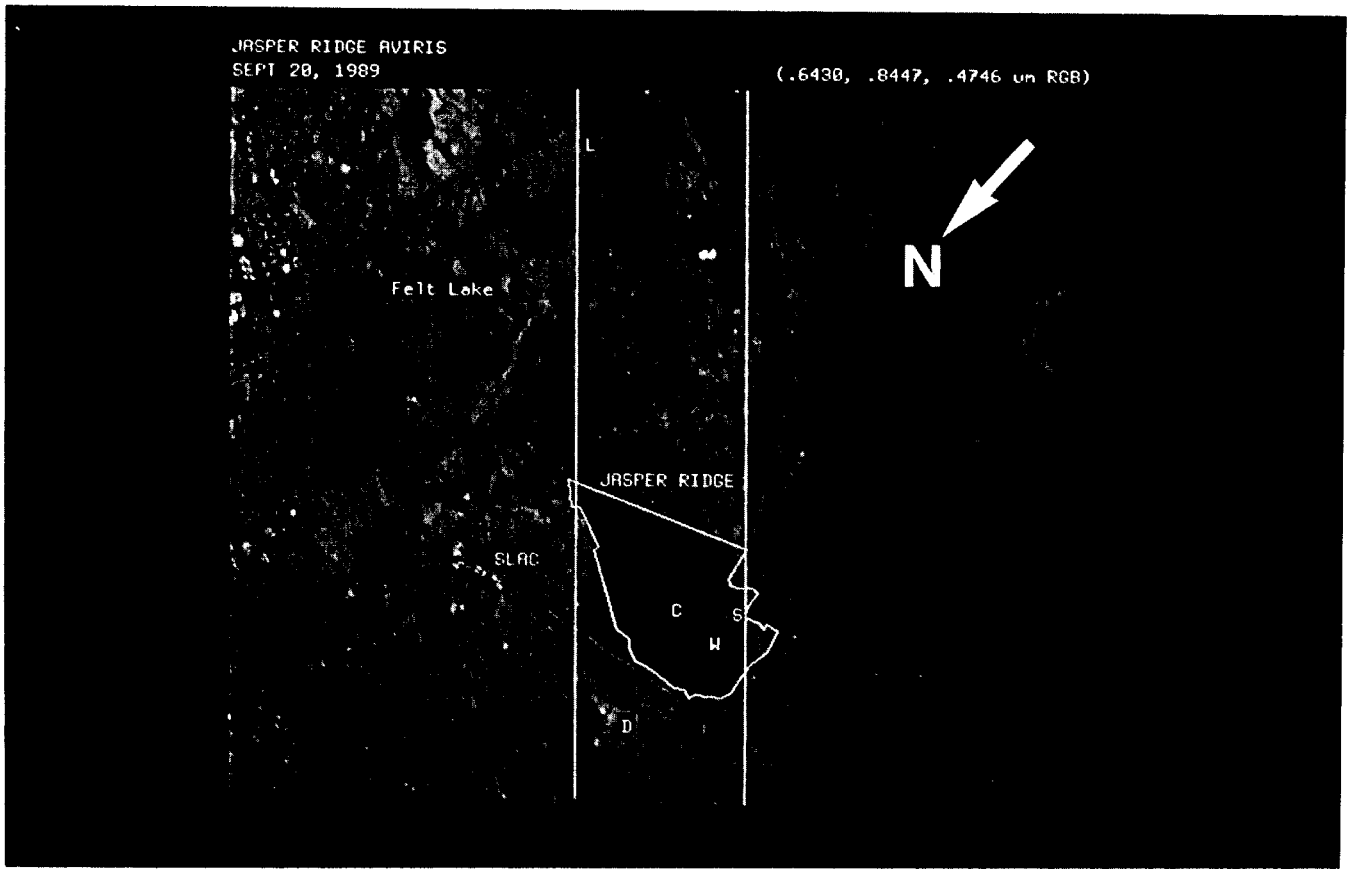

Figure 3. False color composite of AVIRIS data showing the Preserve and the 112-pixel swath. L, C and D are defined in text. S and W are swamp and water respectively.

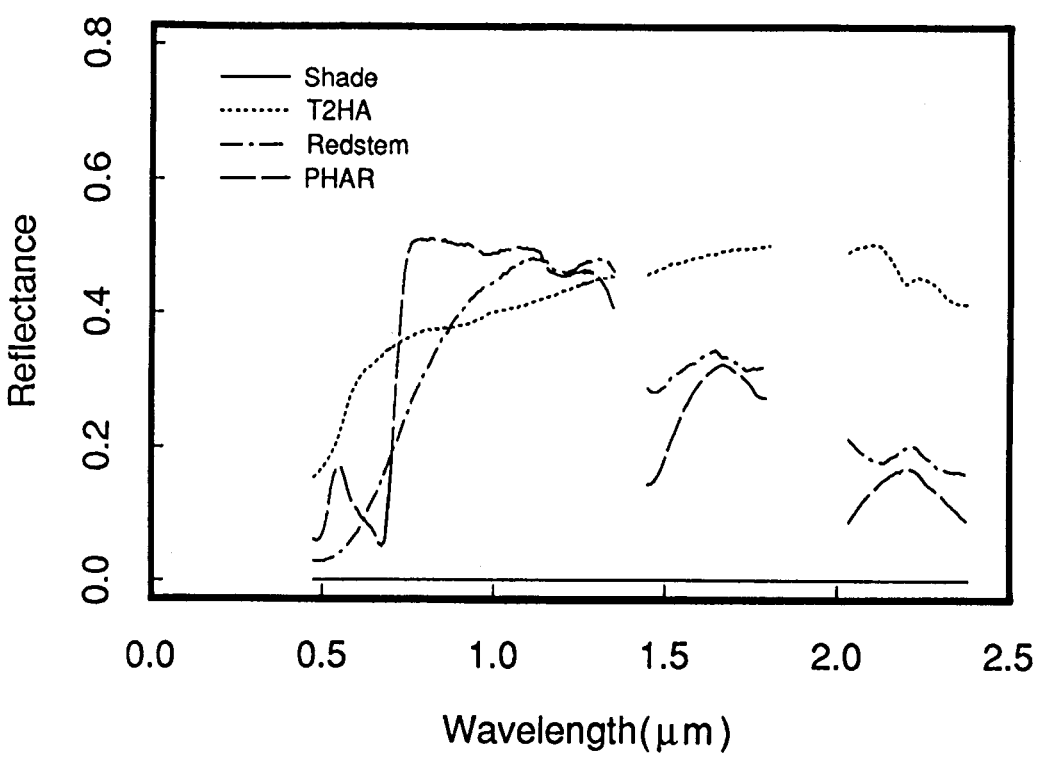

Figure 4. Reflectance spectra of the four endmembers: Shade, T2HA, Red stems and PHAR.

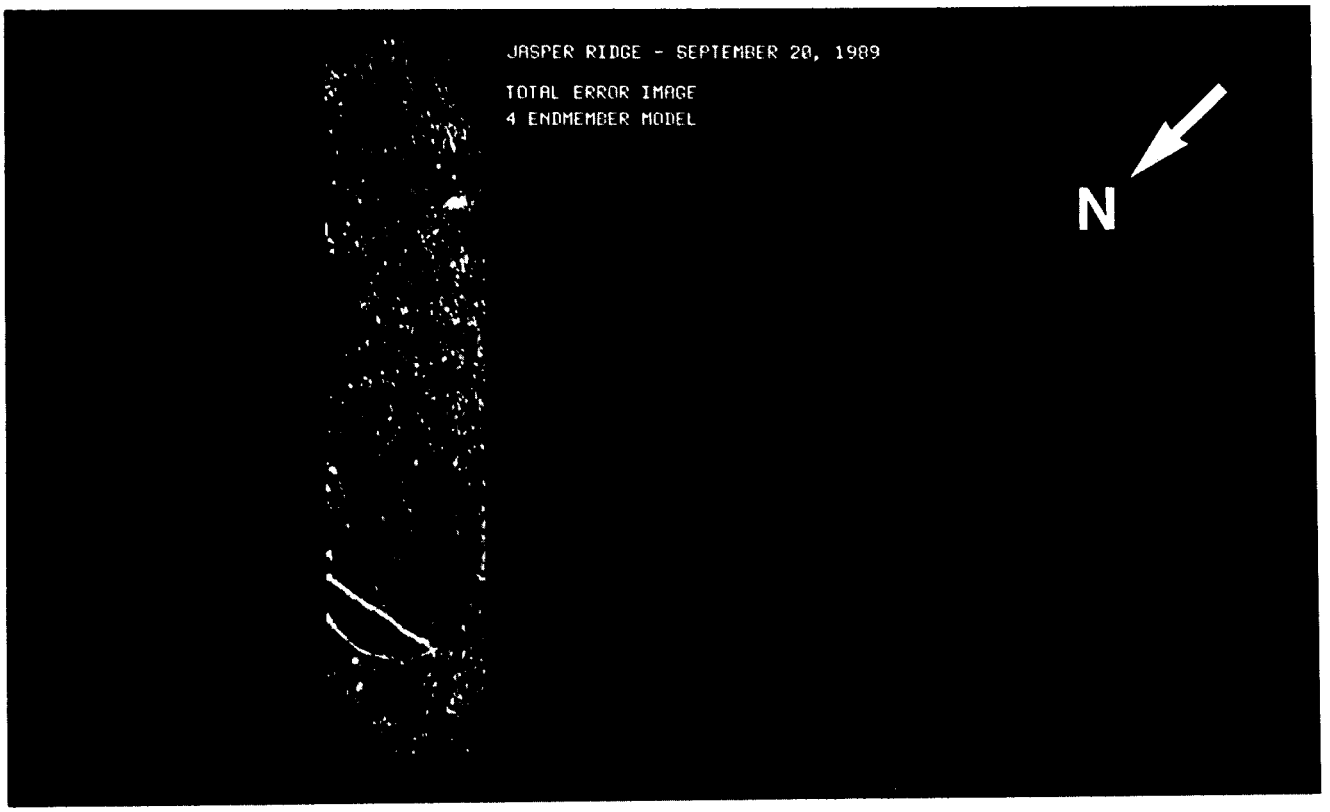

Figure 5. RMS error image. Grey areas indicate good fit of the model (< 2 DN). Light areas have RMS > 3 DN because they were not modeled. The average RMS was less than 3 DN.

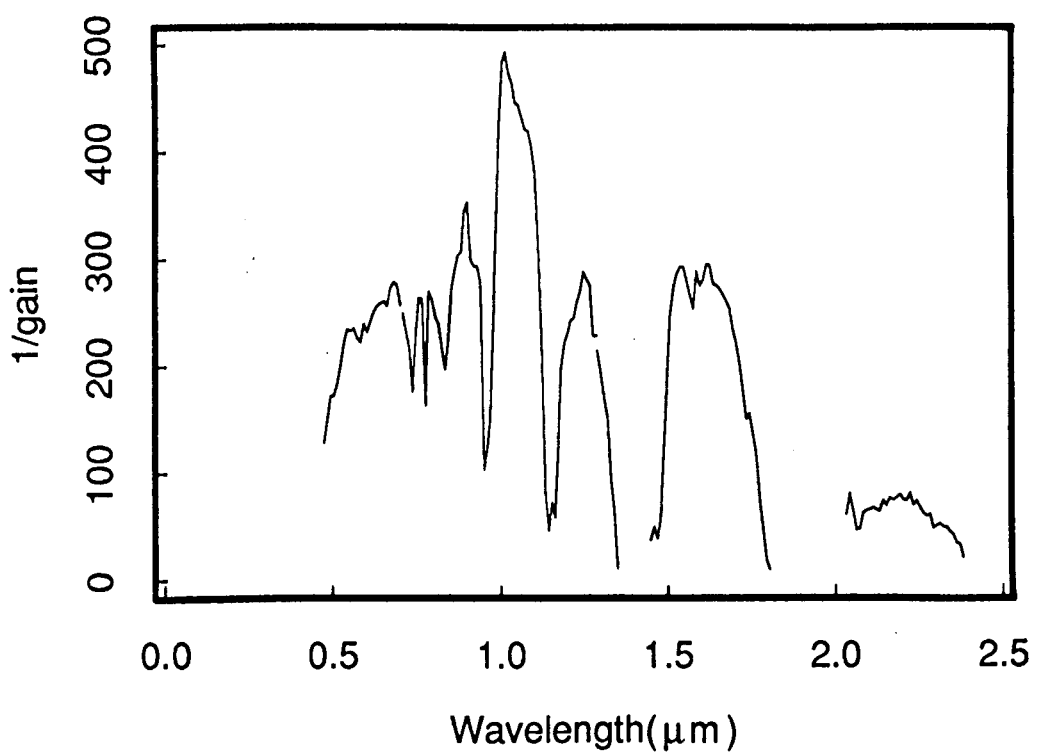

Figure 6. Inverted gains used to calibrate the data to reflectance.

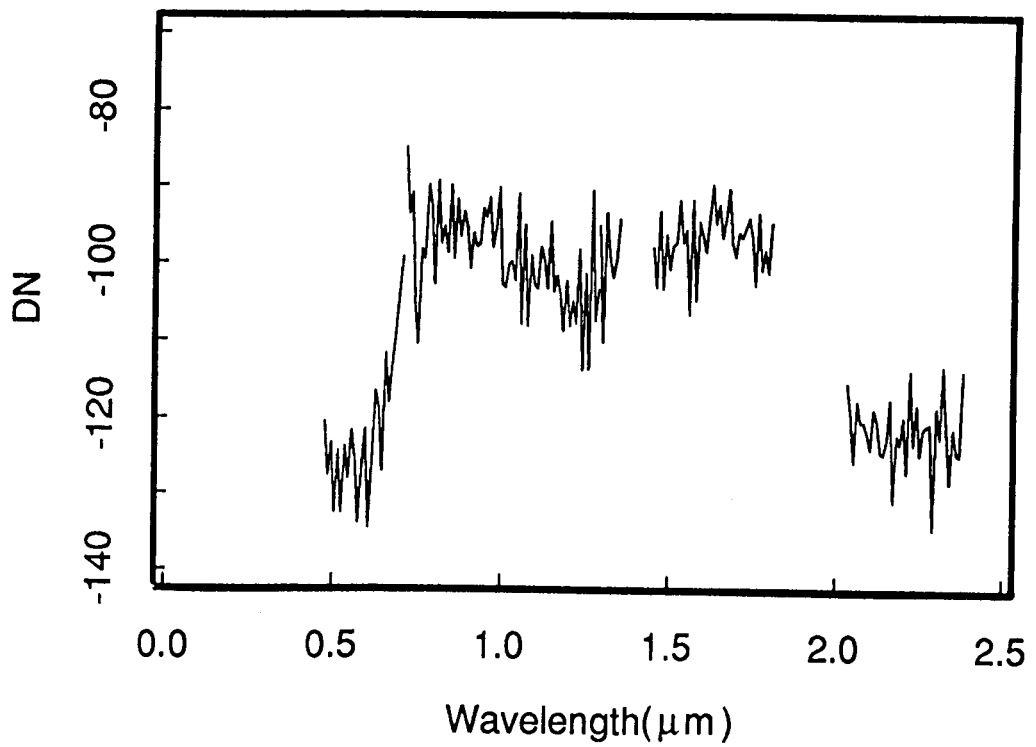

Figure 7. Offsets used to calibrate the data to reflectance.

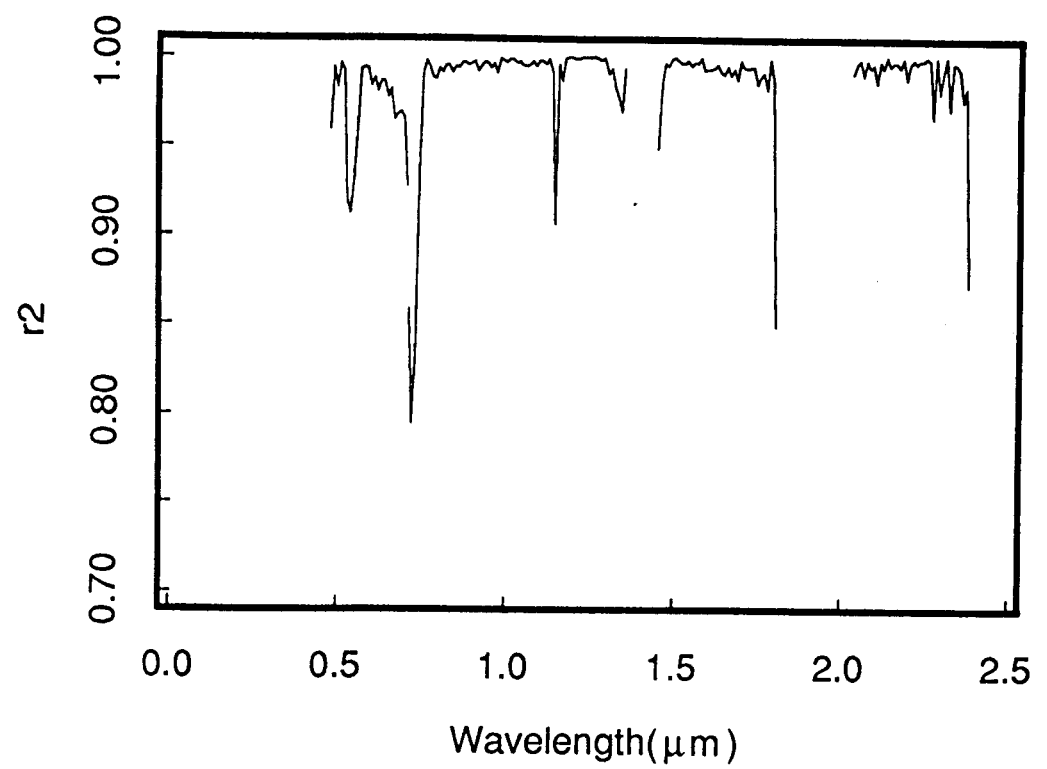

Figure 8. Regression coefficient (r^2) values plotted against wavelength.

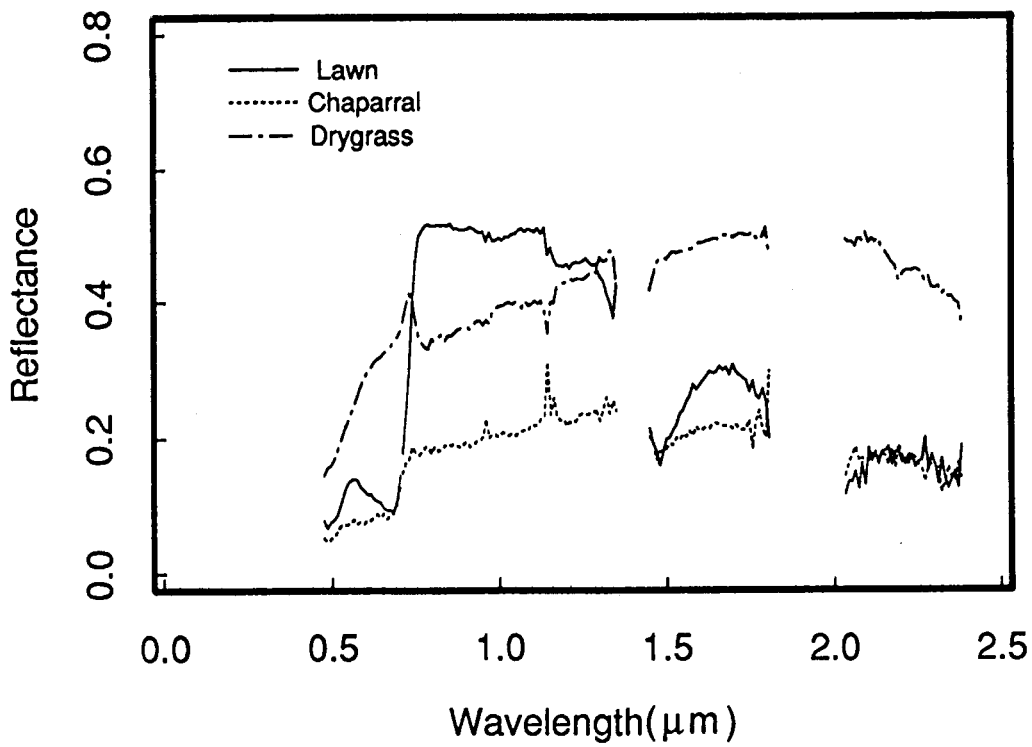

Figure 9. Reflectance spectra from calibrated AVIRIS data. The locations of lawn, chaparral and drygrass are shown on Figure 3, labeled as L, C and D respectively.

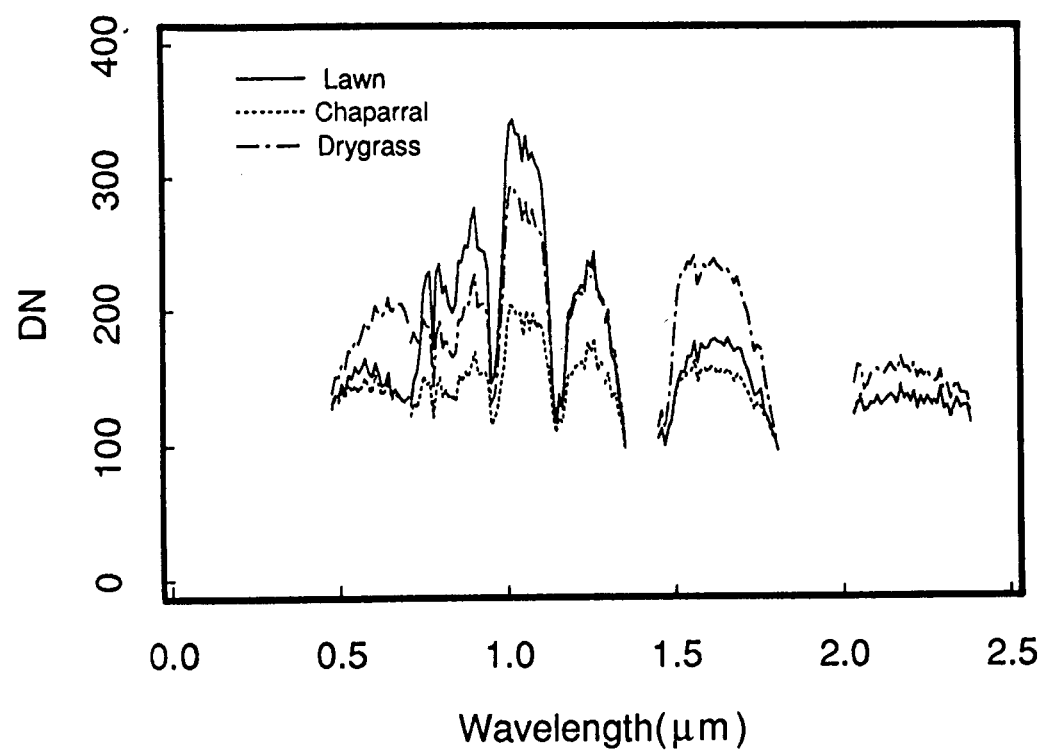

Figure 10. Uncalibrated AVIRIS data for the same areas shown in Figure 10.

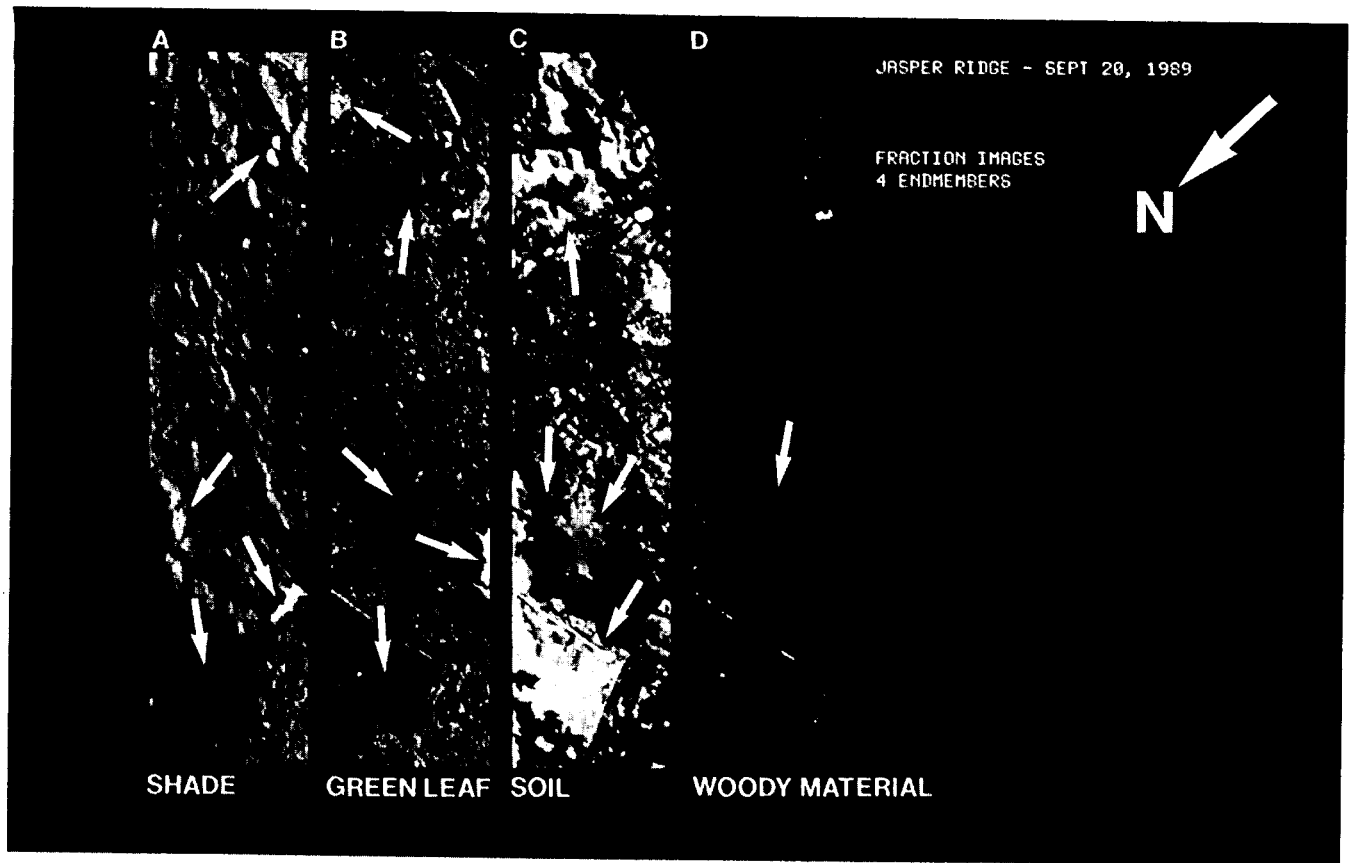

Figure 11. Fraction images of: A) shade, B) green leaf, C) soil, D) woody material.

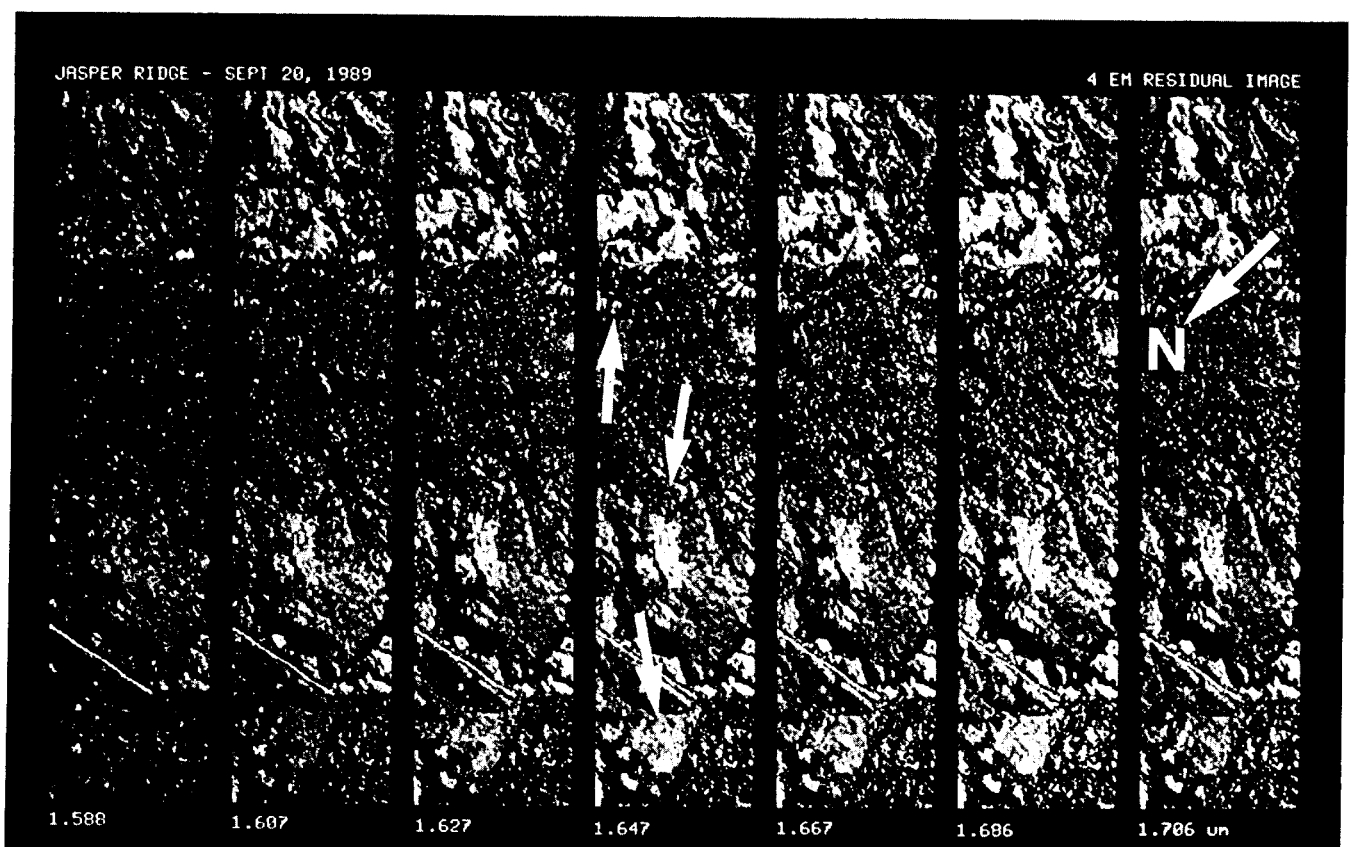

Figure 12. Band residual images for the 1.58 to 1.7 μm region. Light pixels correspond to areas in which the measured spectrum had higher reflectance than the modeled spectrum.

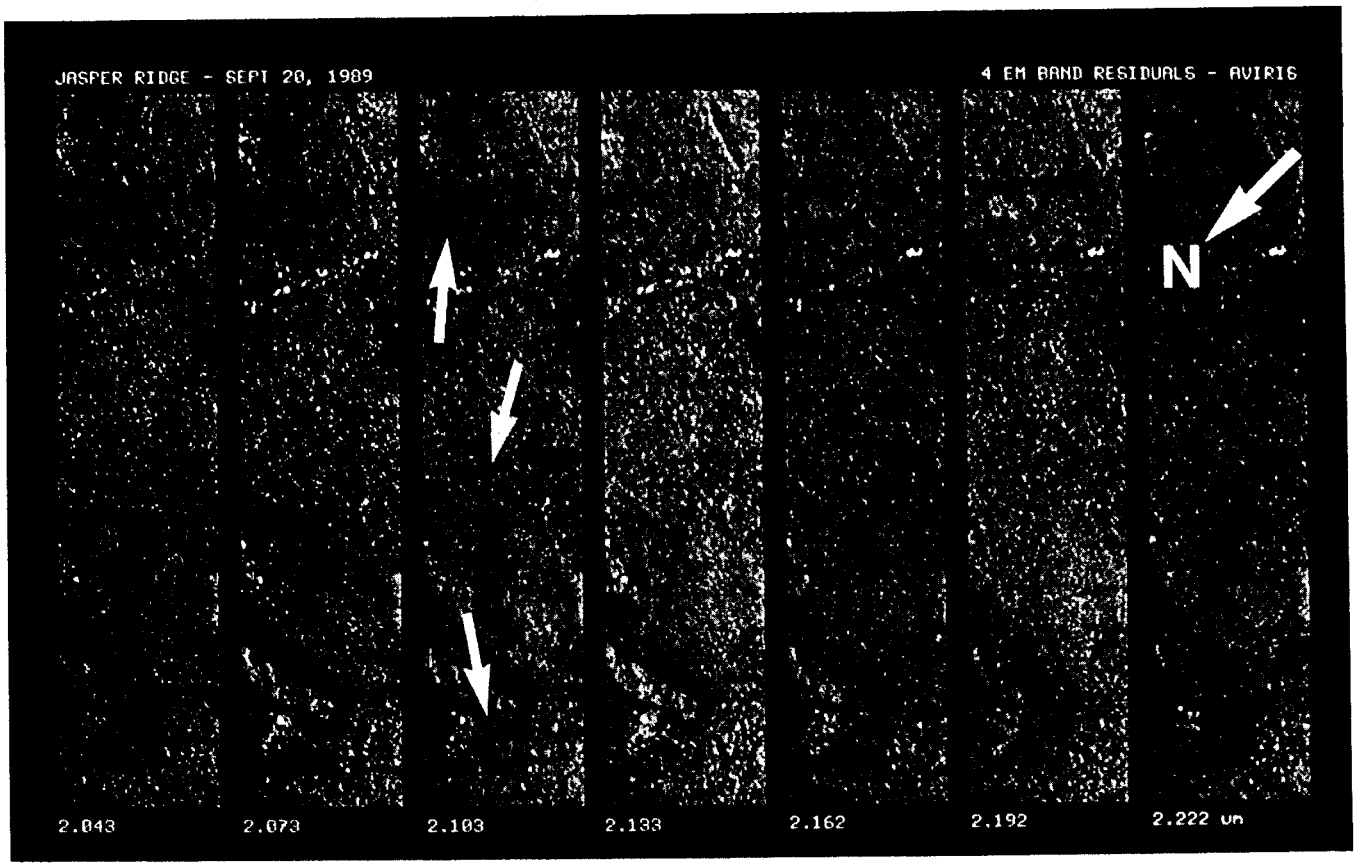

Figure 13. Band residuals for the 2.04 to 2.22 μm region. Dark areas to the north of Jasper Ridge show absorption features lacking in the modeled spectrum.

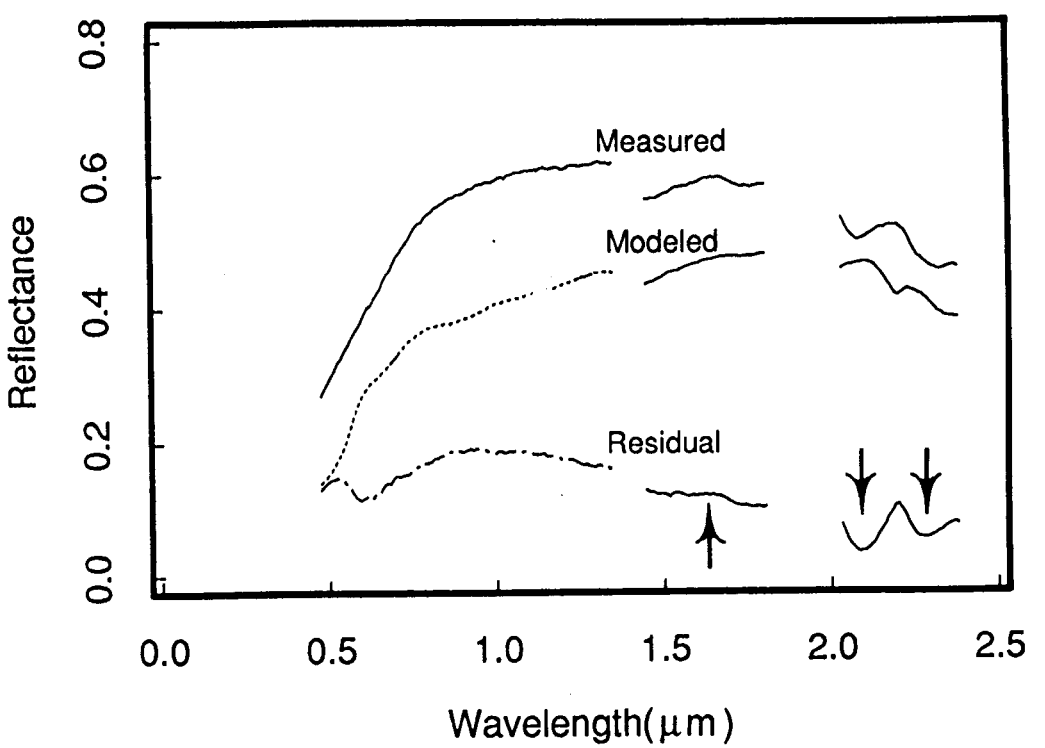

Figure 14. Comparison of measured reflectance spectrum of senescent grass (Phalaris arundinacea) to the linear model of drygrass. The band residual shows subtle spectral highs at 1.55 and 1.64 μm and prominent spectral lows at 2.083 and 2.29 μm (arrows on figure).